Different roles of phosphorous in the nucleation of lithium aluminosilicate glasses

Pauline Glatz[a,b,c,*], Monique Comte[a], Laurent Cormier[b], Lionel Montagne[c], Bertrand Doumert[d], Galan G. Moore[e]

[a] *Corning European Technology Center, 7 Bis Avenue de Valvins, 77210 Avon-France*
[b] *Sorbonne Université, CNRS, Museum National d'Histoire Naturelle, IRD, Institut de Minéralogie, de Physique des Matériaux et de Cosmochimie (IMPMC), UMR 7590, 4 place Jussieu, 75005 Paris, France*
[c] *Univ. Lille, CNRS, Centrale Lille, ENSCL, Univ. Artois, UMR 8181 - UCCS - Unité de Catalyse et Chimie du Solide, F-59000 Lille, France*
[d] *Univ. Lille, CNRS, INRA, Centrale Lille, ENSCL, Univ. Artois, FR 2638 - IMEC - Institut Michel-Eugène Chevreul, F-59000 Lille, France*
[e] *Corning Incorporated, Corning, New York 14831, USA*

Abstract

Glasses in the Li_2O–Al_2O_3–SiO_2 (LAS) system with different $\frac{Al_2O_3}{Li_2O}$ ratio with or without addition of P_2O_5 have been synthesized and characterized by thermal analysis. The glass structure and the phosphorous environments in the glasses and their evolutions with annealing have been studied by ^{31}P Solid-State Nuclear Magnetic Resonance (SSNMR) and 31P/27Al D-HMQC (Dipolar Hetero-nuclear Multiple-Quantum Coherence) correlation NMR. The crystallization behavior has been studied by XRD, SSNMR and RAMAN spectroscopy. The results showed a different role for P_2O_5 depending on the $\frac{Al_2O_3}{Li_2O}$ ratio. For low alumina content, P_2O_5 plays a nucleating role while it acts as crystallization inhibitor for high alumina content. These different roles are related to different local environments of the phosphorus in the as-cast glasses. Our study emphasizes the importance of POAl complexes in the crystallization process of aluminosilicate glasses.

Keywords: P_2O_5, Glass structure, Glass-ceramics, Thermal Analysis, NMR spectroscopy

*Author to whom correspondence should be addressed. e-mail: pauline.glatz@upmc.fr

1. Introduction

Glass-ceramics are materials obtained by controlled crystallization of glasses, which is achieved by thermal heat treatment on parent glasses. [1] The lithium aluminum silicate (LAS) ternary system is one of the most studied and a large number of materials with this composition are commercialized due to their excellent thermo-physical properties. As typical examples we can mention: the near-zero thermal expansion property for β-quartz solid solution glass-ceramics used for telescope mirror, stove cooktops and firedoor applications [2, 3], or the good mechanical properties for compositions with low amount of Al_2O_3 used in the field of restorative dentistry [4]. Since the properties of the glass-ceramics are widely dependent of the nature and relative amount of crystalline phases, the control of nucleation is a key step in order to optimize the final properties. To promote bulk crystallization and obtained an uniform distribution of crystals in the material, nucleating agents such as TiO_2, ZrO_2, and P_2O_5 are typically added in the Li_2O–Al_2O_3–SiO_2 (LAS) glass composition. [5, 6, 7]. In particular, phosphorous, which is classified as a typical network former in glasses, has a complex structural role that strongly impacts its solution behavior, the melt viscosity [8] or its ability to promote liquid-liquid phase separation and affect the crystallization mechanisms [9].

In a study on the effect of the $\frac{Al_2O_3}{M_2O}$ ratio (where M=Li,Na) on the crystallization of LAS system with P_2O_5 addition [10], different crystalline phases were reported depending on the Al_2O_3 content and volume crystallization was observed at low Al_2O_3 amount contrary to surface crystallization observed at high alumina content. Indeed, P_2O_5 is a well-known nucleating agent for low alumina LAS compositions, yielding to $Li_2Si_2O_5$ crystallization. [5, 11, 12, 13, 14] In terms of nucleation mechanism, Headley and Loehman [15] reported that lithium orthophosphate Li_3PO_4 crystals act as heterogeneous nuclei for silicate crystalline phases (metasilicate Li_2SiO_3 and disilicate $Li_2Si_2O_5$ phases). Successive studies using solid state ^{31}P MAS-NMR gave insight on the changes around phosphorous occurring during the crystallization processes [16, 17, 18].

Indeed, MAS-NMR techniques probe the local environment around phosphorus and reveal modifications occurring in the first crystallization steps which could conceivably be missed by other techniques [19]. On a disilicate (aluminum-free) glass-ceramic composition, Holland et al [16] reported that crystalline Li_3PO_4 was not detected by MAS-NMR before the formation of $Li_2Si_2O_5$ phases. However, recent studies revealed that a highly disordered Li_3PO_4 phase is formed concomitantly with Li_2SiO_3 crystallization [17][18].

In aluminosilicate glasses, MAS-NMR showed that phosphorus has different environments depending on the $\frac{Al_2O_3}{M_2O}$ ratio [20][21]. At low P_2O_5 content, a majority of ${PO_4}^{3-}$ orthophosphate and ${P_2O_7}^{4-}$ pyrophosphate groups are observed in the glass matrix, while for increasing Al_2O_3 contents, aluminophosphate groups are formed. Recent developments in NMR provide information on the connectivity of PO_4 tetrahedra with the aluminosilicate network. Spatial proximities between P and Al were reported in systems with low amount of P_2O_5 and Al_2O_3 [22][23] and aluminophosphate groups could be detected in such glasses. Nevertheless, such methods were not used up to now for the detailed study of the nucleation process by P_2O_5 in LAS glass-ceramics. The aim of the present work is to provide new insights to elucidate the role of phosphorous in crystallization mechanisms of LAS compositions with different $\frac{Al_2O_3}{Li_2O}$ ratio. We report a combination of characterization and spectroscopic methods to investigate the crystallization sequences and the nucleating role of phosphorous. NMR and Raman spectroscopies enable us to discuss the changes in the phosphorus environments in relation with the crystallization processes, showing a different behavior between the glasses containing low and high Al_2O_3 contents.

2. Experimental Section

2.1. Materials

Glasses were prepared in the Li_2O-Al_2O_3-SiO_2 (LAS) ternary system with addition of P_2O_5 oxide as a nucleating agent. Analytical grade precursors (Li_2CO_3, Al_2O_3, SiO_2 and $(NH_4)_2HPO_4$) were ground together, dried and

melted in a Pt crucible at 1550°C for 2 h, then quenched by immersing the bottom of the crucible into water. The glasses were ground and molten once again to ensure a good homogeneity. Table 1 reports the glass compositions. They are located along the 74 mol% SiO_2 isopleth, with 0 or 1 mol% P_2O_5. These compositions cover a range with a ratio R=$\frac{Al_2O_3}{Li_2O}$ from 0 (Al-free) to 1.3 (peraluminous composition). The glasses are labeled as follow: LASR-Pn, where R is the ratio $\frac{Al_2O_3}{Li_2O}$ and n the mol% of P_2O_5. Transparent, bubble free, glasses were obtained excepted for the LAS0-P1, which is opalescent. For all samples, powder XRD patterns show the characteristic broad peak of amorphous materials and no Bragg peak. The glass compositions were checked by Electron probe micro-analyser (CAMPARIS, Paris, France) with a CAMECA SX-Five apparatus (15 kV, 10 nA) for SiO_2, Al_2O_3, P_2O_5 and by a Flame-Atomic Absorption Spectrometer in emission mode (Agilent, AA280FS) for Li_2O content.

2.2. Differential scanning calorimetry

Differential Scanning Calorimetry (DSC) thermograms were recorded on a 404 C Pegasus calorimeter from Netzsch (Selb, Germany). All the measurements were carried out in air and heat treatments were conducted at 10°C/min with a bulk sample of ∼50 mg in Pt crucible, using an empty Pt crucible as reference. The crystallization temperature of the first exothermic event was determined at the maximum of the peak. The glass transition temperatures T_g, the onset crystallization temperatures T_x and the temperatures of the maximum of the first crystallization peak T_c are reported in Table 1.

2.3. XRD

X-ray diffraction was carried out at room temperature using a diffractometer (PANalytical X'Pert PRO) with Ni-filtered CuKα radiation (λ =1.5418 Å). Data were recorded in the 10°≤2θ ≤80°range with a step increment of 0.016 °and an interval time of 0.82 sec per step.

2.4. RAMAN spectroscopy

Raman spectra of the glasses and annealed glasses were obtained using a Horiba LabRam HR Evolution system with Ultra-Low Frequency (ULF) module, 1800 gr/mm grating, and a 532 nm laser operating at 100 mW. A x10 magnification objective was used for this study. Each sample was analyzed with an exposure time of 30 sec (per window) with 10 accumulations and a spectral window from 5 to 2000 cm^{-1}. No temperature correction nor normalization have been used for these spectra.

2.5. Scanning Electron Microscopy

Scanning Electron Microscopy (SEM) was used to observe the microstructure of the samples. Bulk glass pieces were embedded in epoxy resin, then cross sections were polished and etched with 1 mol% HF for 30 seconds. They have been coated with iridium (2 nm thick) and observed using a SEM-FEG (Field Emission Gun) ZEISS LEO 1550 (Jena, Germany), at a 5 kV accelerating voltage. Observations have been done with the In-lens secondary electrons detector.

2.6. Solid-state NMR

^{31}P and ^{27}Al MAS-NMR (Magic Angle Spinning Nuclear Magnetic Resonance) spectra were recorded at 9.4 and 18.8 T on Bruker AVANCE I and AVANCE III spectrometers, respectively, with a 4 mm probe at 12.5 kHz spinning speed for ^{31}P and a 3.2 mm probe at 20 kHz spinning speed for ^{27}Al. The Larmor frequencies were 161.9 and 208.5 MHz for ^{31}P and ^{27}Al, respectively. For ^{31}P, the pulse duration was 4.8 μs ($\pi/2$), and the recycle delay (rd) was 120 s. For ^{27}Al, the pulse duration was 1 μs ($\pi/10$), and the rd 2 s. The recycle delays have been defined to enable enough relaxation to get quantitative spectra. The ^{31}P chemical shifts are relative to 85% H_3PO_4 solution at 0 ppm and those of ^{27}Al are referred to $Al(NO_3)_3$ solution as 0 ppm. Decomposition of NMR spectra was done by using dmfit software[24]. The $^{27}Al/^{31}P$ 2D maps were edited with the dipolar heteronuclear multiple quantum coherence (D-HMQC)

sequence [22] on a 18.8 T spectrometer with a 3.2 mm HPAl probe operating at a spinning frequency of 20 kHz. The 988×23 datas points and 3988×19 for LAS0.2-P1 and LAS0.7-P1 samples, respectively, were acquired with a ^{27}Al selective 90°-τ-180°-τ spin-echo. The ^{31}P channel was irradiated with 90 °pulses and with a 1.1 ms recoupling time with the $SR4_1^2$ sequence. Each t1 was recorded with 16384 scans for LAS0.2-P1 (18432 for LAS0.7-P1) with a rd of 0.5 s.

3. Results

3.1. Study of the crystallization

3.1.1. DSC investigations

Figure 1 shows the DSC curves obtained during heating of the glasses with and without P_2O_5 and for different alumina contents. These curves show an endothermic shift of the baseline, which is characteristic of the glass transition (T_g). The increase in T_g when R ratio increases can be attributed to the polymerization of the aluminosilicate glass network. The crystallization of the glasses is revealed by exothermic peaks, which are more or less intense and broad as will be discussed hereafter. We observe two different crystallization behaviors depending on the R ratio: for low alumina content, R<0.7, crystallization peaks are sharper and they appear at lower temperature in glasses with P_2O_5 than those without P_2O_5. For the composition with R=0.2, the DSC curve of the glass with P_2O_5 shows two crystallization peaks, located at 646 °C and 740 °C. These crystallization events are at lower temperatures compared to the glass without P_2O_5, which exhibits a single crystallization peak at 770 °C. These observations are consistent with those on other glasses from the literature, designed to form lithium disilicate glass–ceramics in the SiO_2–Al_2O_3–Li_2O–K_2O–ZrO_2–P_2O_5 system [11]. For R≥0.7, crystallization peaks are observed at higher temperatures for the glasses with P_2O_5, compared to those without P_2O_5. In addition, large crystallization exotherms (i.e. large ΔT, where ΔT is the width of the crystallization exotherm) are observed both with and without P_2O_5. The complete attribution of the different exother-

mic events is beyond the scope of this paper. The parameter $\Delta T_x (=T_x - T_g)$, reflecting the glass stability (GS) [25], can also be considered. The higher the ΔT_x, the lower the ability of a glass to crystallize. In our case, the exact interpretation is not easy as two crystallization mechanisms can occur: volume crystallization and surface crystallization. However, a different behavior for the glasses containing P_2O_5 is clearly observable: when $R<0.7$, ΔT_x is lower (lower GS) for compositions with P_2O_5 than ΔT_x for compositions without P_2O_5. For $R \geq 0.7$, the opposite effect is observed: the addition of P_2O_5 increases the glass stability. As the role of P_2O_5 is different for low or high alumina content, we will focus our investigation on two glass compositions representative of these two different crystallization behaviors: the LAS0.2-P1 composition corresponding to $R<0.7$ range and the LAS0.7-P1 composition corresponding to $R \geq 0.7$ range.

3.1.2. Crystalline phases detected by XRD and RAMAN analysis

The lack of Bragg peaks in the XRD pattern of the LAS0.2-P1 sample (figure 2a) confirms that the initial glass is amorphous. For the annealed samples, the first Bragg peaks are observed for a treatment at 650 °C for 1 minute and are assigned to lithium metasilicate (Li_2SiO_3, JCPDS No. 29-0829) and lithium disilicate ($Li_2Si_2O_5$, JCPDS No. 70-4856) phases. Then, with further treatment at 650 °C for 1 hour, petalite ($LiAlSi_4O_{10}$, JCPDS No. 83-1470) phase appears, which has a layered structure of ${Si_2O_5}^{2-}$ sheets (like $Li_2Si_2O_5$) linked by Li and Al tetrahedra. A β-quartz phase (JCPDS No. 89-8949) is also observed at this thermal treatment. At 815 °C for 1 hour, a small peak due to Li_3PO_4 (JCPDS No. 15-0760) is detected and β-quartz solid solution (a lithium aluminosilicate phase, β-quartz ss) appears, as evidenced by the shift of the main peak of the β-quartz phase to lower 2θ value. Petalite and Li_2SiO_3 are no more observable. With higher treatment temperature (900 °C, 1 hour), β-spodumene solid solution (β-spodumene ss, JCPDS No. 35-0794) phase appears.

For the LAS0.7-P1 composition (figure 2b), the as-cast glass also shows an amorphous bump, but the crystallization sequence is different for the annealed samples. The first Bragg peak appears at 750 °C for 1 minute and is attributed

to a β-quartz solid solution (JCPDS No. 31-0707). With further annealing at 800°C for 1 minute, peaks characteristic of β-spodumene solid solution (JCPDS No. 35-0794) appears. Li_2SiO_3 (JCPDS No. 29-0829) and Li_3PO_4 (JCPDS No. 15-0760) crystals are observed after 1 hour treatment at 800 °C.

Raman study was performed on the two selected glass and glass-ceramic compositions. No curve fitting or deconvolution of the spectra have been done, since spectra were recorded only to get the signatures of the different amorphous and crystalline phases. In addition, information can be obtained on the phosphorous environment in the glass and its evolution with temperature by looking at the 950 cm^{-1} region, which will be detailed in the next section. Main Raman peaks are assigned in figure 3.

For both glasses in figure 3(bottom), two main regions can be observed. The region between 350-650 cm^{-1} is attributed mainly to bending vibrations of Si-O and Al-O bonds associated with high-membered rings of the aluminosilicate network [26]. The region between 1000-1200 cm^{-1} is attributed to Si-O-Si, Si-O-Al asymmetric stretching vibrations and symmetric $Si-O^-$ stretching vibrations [26].

For the LAS0.2-P1 composition (figure 3a), no sharp bands are observable before treatment at 650 °C for 1 hour. The main sharp bands at 409, 451 and 1104 cm^{-1} on the spectrum for this treatment are attributed to $Li_2Si_2O_5$ crystals [27]. At this temperature, crystallization of Li_2SiO_3 is also observed by the presence of peaks at 607 and 979 cm^{-1}, close to those of pure Li_2SiO_3 (613 and 977 cm^{-1} in [28]). In addition, the band at 488 cm^{-1}, characteristic of petalite crystals [29], is also detected at this temperature. At 740 °C for 1 hour, the presence of a sharp band at 462 cm^{-1} indicates β-quartz crystallization [30]. With further annealing, at 815 °C 1 hour, the shift of the band at 462 cm^{-1} to 479 cm^{-1} indicates the appearance of β-quartz solid solution [30]. At 900 °C 1 hour, the band is shifted to a large band near 488 cm^{-1}, characteristic of the presence of β-spodumene solid solution (close to pure β-spodumene at 492 cm^{-1} in [31]). The crystallization of Li_3PO_4 is evident at high temperature with the sharp peak at 947 cm^{-1} close to that of pure $\gamma-Li_3PO_4$ at 950 cm^{-1} according

to [32].

For the LAS0.7-P1 composition (figure 3b), no sharp bands are observable after annealing at 750 °C 1 minute. The spectrum of heated sample at 800 °C for 1 minute shows the crystallization of β-quartz solid solution with the band at 480 cm^{-1} [30] and the shoulder at 453 cm^{-1} [31]. The apparition of β-spodumene solid solution at the expense of β-quartz solid solution is evident at 850 °C by the shift of the band from 480 to 490 cm^{-1} and by the 192 cm^{-1} band [31]. Li_3PO_4 and Li_2SiO_3 crystallization are observed after a treatment at 800 °C for 1 hour with the sharp bands at 944 cm^{-1} for Li_3PO_4 [32] and 975 and 603 cm^{-1} for Li_2SiO_3 [28].

3.1.3. Microstructure

Figure 4a shows SEM image of the LAS0.2-P1 glass treated at 650 °C for 1 minute. Small holes distributed uniformly can be observed. They are attributed to Li_2SiO_3 crystals observed on the XRD pattern, which are easily dissolved in the HF acid solution used for sample preparation, due to their low polymerization degree (chain-like structure). Figure 4b shows SEM image of the LAS0.7-P1 glass treated at 800 °C for 1 minute. Surface crystallization is visible for this sample (constituted of β-quartz ss and β-spodumene ss according to XRD pattern), while no crystal formation is detected in the bulk.

3.2. Structure of the glasses and glass-ceramics

3.2.1. Structure of as-cast glasses

The ^{31}P MAS-NMR spectra of the two glasses in figure 5a present broad resonances characteristics of the amorphous environment around phosphorous. The spectrum of LAS0.2-P1 shows a resonance at 9.2 ppm assigned to orthophosphate units (PO_4^{3-}) [33]. In addition, a second resonance around 0 ppm can be attributed to pyrophosphates units ($P_2O_7^{4-}$) [16] and possibly PO_4^{3-} species charge compensated by Al^{3+}. Indeed, replacing Li^+ by Al^{3+}, which is more strongly bonded, produces an upfield change in the chemical shift, that means more negative values [34]. In solid solution of crystallized $Na_{3-3x}Al_xPO_4$, Dol-

lase evidenced a change of about 8 to 9 ppm for each additional Al [34]. For the LAS0.7-P1 composition, with a higher alumina content, a single broad resonance is present at -3.5 ppm, shifted to more negative chemical shifts compared to LAS0.2-P1, which is attributed to the presence of more Al^{3+} cations compensating the PO_4^{3-} species [20]. These species containing P-O-Al bonds are called POAl complexes in this study.

The ^{27}Al MAS-NMR spectra of the two glasses are shown in figure 5b. They show a single peak in the region 55-60 ppm, ascribed to aluminum in tetrahedral coordination (Al^{IV}). Owing to the presence of an excess of Li^+ for the charge compensation, Al^{3+} adopts a tetrahedral conformation, as reported in per-alkaline aluminosilicate glasses [35]. In addition, a small peak around 25 ppm for the LAS0.2-P1 is detected and could be due to Al^{V} as it has been detected earlier in per-alkaline-earth aluminosilicate glasses. [36]

In order to confirm the presence of POAl complexes mentioned above in these glasses, ^{31}P-^{27}Al heteronuclear correlation 2D-NMR spectra have been recorded to probe the spatial proximity of these nuclei [23]. For that purpose, ^{27}Al{^{31}P} D-HMQC spectra (figure 6) have been recorded. The two spectra exhibit correlation signals between phosphate and aluminate species indicating that Al(IV)-PO_4 entities are present in the glass, even at low alumina content. The projections of the 2D spectra are sketched as dashed lines in figure 6. They show that the maximum intensity of the correlation is centered at 3.5 ppm in the ^{31}P dimension for the LAS0.2-P1. However, this contribution does not take into account all the information under the curve: POAl complex is not the only entity as shown in figure 5. Two other species: PO_4^{3-} only surrounded by Li^+ at 9.2 ppm and pyrophosphate species $P_2O_7^{4-}$ around 0 ppm are observable and are not affected by the correlation. For the LAS0.7-P1 composition, the maximum is shifted to -3.5 ppm in the ^{31}P dimension. The projection of the correlation (in dashed line on the left figure 6b) and the 1D spectrum are superimposed. This indicates that all the P atoms are affected by the correlation and that they see Al^{3+} atoms in their environment. This implies that all the P units are connected to Al.

Previous studies on sodium aluminosilicate glasses evidenced the presence of POAl complexes [20, 21, 23]. In their study of peralkaline compositions, Toplis and Schaller [20] concluded on the presence of individual PO_4^{3-} tetrahedra linked to the aluminosilicate framework with the replacement of one or two Na atoms by Al atoms. They denoted these species $Na_2(NaAl)PO_4$ and $Na(NaAl)_2PO_4$ where (NaAl) represents one of the four bonds of a Al(IV) charge balanced by sodium ($0.25NaAl^{4+}$). $Na_2(NaAl)PO_4$ is at 7 ppm while $Na(NaAl)_2PO_4$ at -5 ppm. Similarly, in our peralkaline Li-aluminosilicate glasses, we can attribute the resonances at 3.5 ppm and at -3.5 ppm to $Li_2(LiAl)PO_4$ and $Li(LiAl)_2PO_4$, respectively. The latter species is the main contribution for the LAS0.7-P1 composition.

3.2.2. Evolution of the local environment around P with temperature

The ^{31}P MAS-NMR spectra of the glass LAS0.2-P1 and glass-ceramics show differences with thermal treatments (figure 7a). Treatment at 550 °C for 1 hour already induces some modifications of the environment around ^{31}P though this temperature is below the glass transition temperature. The intensity of the contribution near 9.2 ppm increases in intensity and its position is shifted to 9.5 ppm. On the spectrum of the sample treated at 650 °C for 1 minute, the resonance is shifted again to higher chemical shift near 10 ppm and its intensity becomes sharper, indicating the onset of orthophosphate crystallization. Indeed, the chemical shift is close to the chemical shift of pure crystalline Li_3PO_4 (10 ppm) [33]. However, the linewidth of the resonance is still large (∼3 ppm) indicating a chemical shift distribution due to some residual disorder. The persistence of disorder suggests the presence of a poorly crystallized intermediate species. With further thermal treatments at 650 °C, 740 °C, 815 °C and 900 °C for 1 hour, this contribution becomes even sharper and its linewidth decreases to ∼0.8 ppm at 900°C, the same order of magnitude for the linewidth has been observed in the study of Bischoff et al. [17] at high temperature treatment. These modifications reveals the increasing crystallinity of this orthophosphate species (Li_3PO_4). In parallel, the resonances at 3.5 ppm and around 0 ppm decrease

in intensity and almost disappear at 815°C. The only resonance remaining at 900°C is the one at 10.3 ppm, corresponding to crystalline Li_3PO_4 (figure 7a). Theses changes are also consistent with the thermal evolution associated with P environment observed by RAMAN spectroscopy (figure 3a). The intense band near 950 cm^{-1} is assigned to the symmetrical stretching vibration of the P-O bond [37]. For the as-cast glass, this band is broad and located at 957 cm^{-1}. This corresponds to P in the silicate network, mainly in orthophosphate species. With increasing annealing temperatures, the band increases in intensity and becomes sharper and its position is shifted down to 947 cm^{-1}, very close to the band characteristic of $\gamma-Li_3PO_4$ located at 950 cm^{-1} [32]. The shift in position starts at 550 °C for 1 hour treatment, in agreement with the evolution of the local P environment determined by NMR (figure 7a).

For the composition LAS0.7-P1, the ^{31}P MAS-NMR spectra of the glass and the glass-ceramics heat-treated at 700 °C and 750 °C for 1 minute are nearly identical. A peak at 10 ppm attributed to nanocrystalline Li_3PO_4 (linewidth ~1.8 ppm) appears after a treatment at 800 °C for 1 minute, while the contribution around -3.5 ppm is still present. With annealing at 800°C, 850 °C and 900 °C for 1 hour, this peak becomes sharper and its position is shifted to 10.6 ppm (linewidth of ~1.1 ppm). It is the only observable contribution at the end of annealing treatments.

The RAMAN spectra for the LAS0.7-P1 composition (figure 3b) are also in agreement with the evolution observed by NMR. Unlike the LAS0.2-P1 composition, no PO_4^{3-} band is discernible at 957 cm^{-1} in the as-cast glass. The band associated with Li_3PO_4 (944 cm^{-1}) first appears after the 800 °C 1 minute treatment like in the NMR spectrum.

4. Discussion

4.1. Chemical dependence of the crystallization process

The DSC study provided evidence for two contrasting crystallization behaviors of the glasses, depending on their alumina contents. At low alumina

content, addition of P_2O_5 results in DSC peaks that become sharper and located at lower temperatures compared to the glasses without P_2O_5. It is known that for a given heating rate (10 °C/min in all our DSC experiments), a sharp peak (small ΔT) denotes bulk crystallization while a broad peak (large ΔT) is an indication of surface crystallization [38]. SEM analysis (figure 4b) confirms mainly internal crystallization for the LAS0.2-P1 glass (figure 4a). Moreover, the addition of efficient nucleating agents such as TiO_2 and ZrO_2 in some aluminosilicate glasses leads to crystallization peaks at low temperatures [39, 40]. This effect was also observed for P_2O_5 in lithium disilicate-based glass [41, 42], which was explained by more nucleation sites created with the addition of P_2O_5.

For high alumina content R≥0.7, crystallization peaks are broad with or without P_2O_5, suggesting surface crystallization in both cases, which is confirmed by SEM analysis (figure 4b). In addition, T_c is higher with P_2O_5, revealing a delay in crystallization in this glass composition. This suggests an opposite effect of the P_2O_5 compared to the glass with low alumina content. This difference of nucleation efficiency with P_2O_5 has been also evidenced in a previous study [10]. They have observed for a compositionally complex LAS glass with 2.5 wt% P_2O_5 that surface crystallization is favored at high alumina content while volume crystallization is obtained at low alumina content. However, the origin of this difference has not been investigated. To understand this contrasting behavior, we have considered the structural evolution of the local P environment during different annealing treatments. As shown earlier [11] [43], crystalline phases containing phosphate are observed by XRD only for high temperature treatments, whereas NMR and Raman spectroscopies are able to detect subtle variations at much lower temperature, even in the T_g range. This is because XRD necessitates the organization of large crystallization domains, whereas NMR and RAMAN investigate disordered and ordered local arrangements.

4.2. P_2O_5 as nucleating agent

Upon annealing, important changes of the P environments can be observed with two distinct behaviors for the low and high alumina glass compositions (figure 7). For the LAS0.2-P1 glass, modifications of the P environment is observed for the glass heat treated at 550 °C for 1 hour (figure 7a), i.e. prior to the detection of any crystallization with XRD (figure 2a). This suggests that some structural relaxation takes place, which corresponds to a structural reorganization around phosphorous atoms. Raman analysis (figure 3a) confirms this initial reorganization around P.

In the sample heat treated at 650 °C for 1 minute, the orthophosphate contribution is shifted towards high chemical shift values and its intensity becomes sharper, indicating that P atoms evolves towards an environment consistent with the formation of crystalline Li_3PO_4 but not well crystallized, as the linewidth is large compared to pure Li_3PO_4. This species appears concomitantly with the crystallization of the first phases detected by XRD (Li_2SiO_3 and $Li_2Si_2O_5$ in our study). This disordered Li_3PO_4 has been suggested as an intermediate nucleation step in previous crystallization investigations for non stoichiometric disilicate glasses [17][18]. In these studies, a strongly disordered P-containing phase appears first with Li_2SiO_3 crystallization while well-ordered crystalline Li_3PO_4 appears at higher temperature together with the formation of $Li_2Si_2O_5$ [17][18].

Similarly, annealing of the LAS0.2-P1 glass at higher temperatures (650 °C 1h, 740 °C 1h and 815 °C 1h) lead to an increase of the ordering around P as indicated by the sharpening of the NMR resonance at 10 ppm. This is accompanied by the disappearance of the pyrophosphate $Li_4P_2O_7$ and $Li_2(LiAl)PO_4$ species. After annealing at 900 °C for 1 hour, the only contribution is at 10.3 ppm, attributed to well-crystallized Li_3PO_4 and Bragg peaks characteristics of this phase are observed by XRD.

^{31}P MAS-NMR spectrum for the LAS0.2-P1 glass show that the monomeric ${PO_4}^{3-}$ and dimeric ${P_2O_7}^{4-}$ units are essentially present in the as-cast glass, surrounded by Li^+ ions to ensure charge compensation of the tetrahedral units. An ascertained role of P is to promote phase separation in glasses [9]. However,

it is difficult to conclude if the PO_4^{3-} tetrahedra are isolated from each other or if they tend to segregate within the silicate network. Using an advanced NMR technique (^{31}P spin-counting), Fayon et al. [44] have shown that nanometric-sized heterogeneities can be evidenced in a lime phosphosilicate bioactive glass with phosphate clusters containing 5-6 PO_4^{3-} entities. A similar approach appears unsuccessful in our glass since we have measured that the relaxation time is too low (<7 ms) compared to the one (around 20 ms) required to probe P-P connectivities with this technique.

Although the glass studied is transparent and no phase separation is observable by SEM, nano-heterogeneities in terms of P-enriched nano-domains could still be present. Indeed, Dargaud et al. [45] evidenced nano heterogeneities by electron microscopy of 1-5 nm for a MgO-Al_2O_3-SiO_2 glass with ZrO_2 addition though the glass is transparent and appears as amorphous by XRD. Interestingly, during the first annealing treatments, the P environment evolves towards the formation of disordered Li_3PO_4 domains. Locally, these clusters correspond to Li^+ ions scavenged by the phosphorous atom and a remaining silicate network depleted in Li^+ ions and, thereby, more polymerized. This is confirmed by Bischoff et al. [17], who evidenced by a ^{29}Si/^{7}Li NMR correlation technique a lithium clusterization before crystallization of Li_2SiO_3. These disordered orthophosphate clusters embedded in the silicate network have two possible effects on the crystallization mechanism. First, the crystallization of silicate phases is possible due to lowering interfacial energy resulting from a high concentration of Li atoms and a low polymerization of the silicate network close to Li- orthophosphate clusters. These compositional and structural fluctuations should promote the formation of Li_2SiO_3. This scenario explains the proximity of the silicate phases and Li_3PO_4 and corresponds to the epitaxial growth observed in a early study by Headley and Loehman [15]. Alternatively, the orthophosphate heterogeneities are embedded in a silicate network whose composition is shifted towards the center of the Li_2O-SiO_2 immiscibility dome. This could promote phase separation between Li-rich regions and Si-rich regions, not necessarily associated with the orthophosphate domains. Again, such liquid-liquid phase

separation could favor homogeneous nucleation of silicate phases. In both cases, internal crystallization is achieved.

4.3. P_2O_5 as inhibitor of crystallization

In the case of the LAS0.7-P1 composition, the ^{31}P MAS-NMR spectra of glasses annealed at 700 °C and 750 °C for 1 minute show very little variation compared to the as-cast glass (figure 7b). The first important modification in the NMR spectra appears after annealing at 800 °C for 1 minute, that is after the first crystallization observable by XRD at 750 °C for 1 minute. At 800 °C, a peak at 10 ppm appears due to nanocrystalline Li_3PO_4 while the contribution $Li(LiAl)_2PO_4$ is still present. In the RAMAN spectra in figure 3b, the two first modifications appear simultaneously at 800 °C: the main band characteristic of β-quartz ss and the one due to Li_3PO_4. Both NMR and RAMAN agree that no rearrangement around P is observed before crystallization of the LAS0.7-P1 glass, contrary to LAS0.2-P1. When crystallization of Li_3PO_4 occurs, POAl complexes are no more detected in the NMR spectra.

In the LAS0.7-P1 composition, the nanocrystalline Li_3PO_4 appears after crystallization of the aluminosilicate network and this is not preceded by a reorganization of the P environment. This indicate that for the Al-rich compositions, P does not play an active role in the crystallization process, which explains that surface crystallization mainly occurs. A nucleating role for P is likely inhibited by the formation of POAl complexes. Though spatial proximities between P and Al is revealed by the ^{27}Al$\{^{31}$P$\}$ D-HMQC correlation technique for the two compositions with low and high alumina content, the POAl complexes are present in a minor amount in LAS0.2-P1 NMR spectra at 3.5 ppm. The POAl complexes present for low alumina content strongly suggests a preferential association of these two cations. For the LAS0.7-P1 glass (figure 6b), the component attributed to POAl complexes is clearly predominant (at -3.5 ppm) and no PO_{43}^{-} tetrahedra surrounded only by Li^+ or $P_2O_7^{4-}$ can be detected. This indicates that addition of P_2O_5 results in the incorporation of PO_4^{+} tetrahedral units within the aluminosilicate network. Due to the Al avoidance rule, few Al-O-Al

bondings are expected and Al atoms are dispersed within the polymeric network of alkali aluminosilicate glasses [46][47]. Consequently, phosphorus atoms are likely well-separated within the aluminosilicate network due to their bonding with Al. Such network organization prevents the formation of phosphate clusters and the formation of Li-rich zones, contrary to LAS0.2-P1. Furthermore, PO_4^+ sites are stabilized as charge balance is ensured by AlO_4^- tetrahedra [48]. The formation of P-O-Fe^{3+} complexes in silicate melts was also proposed to hinder the crystallization of magnetite [49].

In addition, T_c peaks (Figure 1) appears at lower temperatures in LAS0.7-P0 compared to LAS0.7-P1 indicating that P_2O_5 mitigates the surface crystallization of β-quartz ss. P_2O_5 plays no role in bulk crystallization but affects in another way the crystallization of this glass by stabilizing the glass structure. Others studies concluded on this dual role of P_2O_5 depending the composition in SrO–TiO_2–Al_2O_3–SiO_2–B_2O_3 system [50]. In addition, in a Na_2O-2CaO-$3SiO_2$ glass, addition of 2 wt% of P_2O_5 enhances glass-forming tendency by diminishing nucleation rate[51].

5. Conclusions

Compositions from the LAS system with different $R = \frac{Al_2O_3}{Li_2O}$ ratio and with P_2O_5 have been investigated. Thermal analysis showed a distinct crystallization behavior for low and high alumina content. 2 compositions were selected with low and high alumina content, and phase evolution and environment around phosphorus have been explored, as well as their modification after thermal treatments at different temperatures. This work reveals two distinct roles of P_2O_5 depending on the presence of POAl complexes: easier bulk crystallization is obtained for the R=0.2 composition, indicating a nucleating role for P_2O_5, while higher crystallization temperatures are observed for the R=0.7 composition, suggesting that P_2O_5 enhances glass stability. The POAl complexes could be detected even with low alumina content thanks to the enhanced sensitivity of the D-HMQC NMR pulse sequence. The nucleating role of P_2O_5 is not related

to the crystallization of lithium orthophosphate phases, as these crystals appears after the crystallization of lithium silicate phases. The presence, and development upon annealing, of structurally disordered heterogeneities associated with P is responsible for changes in structure and properties of the remaining glass, which promotes crystallization at low alumina content. With increasing Al_2O_3 content, the POAl complexes become the dominant species. These complexes result in the dispersion of phosphate species within the glass matrix and prevent the formation of the heterogeneities associated with P. As a consequence, P_2O_5 can be considered as a crystallization inhibitor in LAS glasses with high alumina content.

Acknowledgments

We would like to acknowledge Anne Crochet (CETC Corning) for SEM images, Peggy Georges and Sandrine Bercy (CETC Corning) for chemical analysis. We thank also Laurent Delevoye for fruitful discussions. The ANRT is acknowledged for PhD funding (P.G.) under the CIFRE Contract 2015/0529. The authors thank the Chevreul Institute (FR 2638) for its help in the development of this work. Chevreul Institute is supported by the « Ministère de l'Enseignement Supérieur et de la Recherche », the « Région Nord-Pas de calais » and the « Fonds Européen de Développement des Régions ».

References

[1] W. Höland, G. H. Beall, Glass-ceramics technology, Wiley-American Ceramic Society, 2012.

[2] G. H. Beall, L. R. Pinckney, Nanophase glass-ceramics, J. Am. Ceram. Soc. 82 (1) (1999) 5–16.
URL http://onlinelibrary.wiley.com/doi/10.1111/j.1151-2916.1999.tb01716.x/full

[3] M. Comte, Commercial applications of glass-ceramics, in: From glass to crystal, EDP Sciences, 2017, pp. 361–374.

[4] S. Huang, Y. Li, S. Wei, Z. Huang, W. Gao, P. Cao, A novel high-strength lithium disilicate glass-ceramic featuring a highly intertwined microstructure, J. Eur. Ceram. Soc 37 (3) (2016) 1083–1094. doi:10.1016/j.jeurceramsoc.2016.10.020.
URL http://linkinghub.elsevier.com/retrieve/pii/S0955221916305702

[5] W. Holand, V. Rheinberger, M. Schweiger, Control of nucleation in glass ceramics, Philos. Trans. R. Soc. London, Ser. A 361 (1804) (2003) 575–589. doi:10.1098/rsta.2002.1152.
URL http://rsta.royalsocietypublishing.org/cgi/doi/10.1098/rsta.2002.1152

[6] L. R. Pinckney, G. H. Beall, Microstructural evolution in some silicate glass–ceramics: A review, J. Am. Ceram. Soc. 91 (3) (2008) 773–779. doi:10.1111/j.1551-2916.2007.02129.x.
URL http://doi.wiley.com/10.1111/j.1551-2916.2007.02129.x

[7] E. D. Zanotto, V. M. Fokin, Recent studies of internal and surface nucleation in silicate glasses, Philos. Trans. R. Soc. Lond. A 361 (1804) (2003) 591–613. doi:10.1098/rsta.2002.1150.
URL http://rsta.royalsocietypublishing.org/cgi/doi/10.1098/rsta.2002.1150

[8] M. J. Toplis, D. B. Dingwell, The variable influence of P_2O_5 on the viscosity of melts of differing alkali/aluminium ratio: Implications for the structural role of phosphorus in silicate melts, Geochim. Cosmochim. Acta 60 (21) (1996) 4107–4121.

[9] P. F. James, Liquid-phase separation in glass-forming systems, J. Mater. Sci. 10 (10) (1975) 1802–1825.
URL http://link.springer.com/article/10.1007/BF00554944

[10] A. Arvind, A. K. Tyagi, R. Mishra, V. K. Shrikhande, G. P. Kothiyal, Evolution of crystalline phases as a function of composition and dwell time in lithium aluminium silicate glass-ceramics, Phys. Chem. Glasses-Eur. J. Glass Sci. Technol. B 49 (3) (2008) 166–173.

[11] W. Höland, E. Apel, C. van't Hoen, V. Rheinberger, Studies of crystal phase formations in high-strength lithium disilicate glass–ceramics, J. Non-Cryst. Solids 352 (38) (2006) 4041–4050. doi:10.1016/j.jnoncrysol.2006.06.039.
URL http://linkinghub.elsevier.com/retrieve/pii/S0022309306010052

[12] X. Zheng, G. Wen, L. Song, X. Huang, Effects of P_2O_5 and heat treatment on crystallization and microstructure in lithium disilicate glass ceramics, Acta Mater. 56 (3) (2008) 549–558. doi:10.1016/j.actamat.2007.10.024.
URL http://linkinghub.elsevier.com/retrieve/pii/S1359645407006933

[13] F. Wang, J. Gao, H. Wang, J.-h. Chen, Flexural strength and translucent characteristics of lithium disilicate glass–ceramics with different P_2O_5 content, Mater. Design 31 (7) (2010) 3270–3274. doi:10.1016/j.matdes.2010.02.013.
URL http://linkinghub.elsevier.com/retrieve/pii/S0261306910000865

[14] S. C. von Clausbruch, M. Schweiger, W. Höland, V. Rheinberger, The effect of P_2O_5 on the crystallization and microstructure of glass-ceramics in the SiO_2–Li_2O–K_2O–ZnO–P_2O_5 system, J. Non-Cryst. Solids 263-264 (2000) 388–394. doi:10.1016/S0022-3093(99)00647-X.
URL http://www.sciencedirect.com/science/article/pii/S002230939900647X

[15] T. J. Headley, R. E. Loehman, Crystallization of a glass-ceramic by

epitaxial growth, J. Am. Chem. Soc. 67 (9) (1984) 620–625.
URL http://onlinelibrary.wiley.com/doi/10.1111/j.1151-2916.1984.tb19606.x/full

[16] D. Holland, Y. Iqbal, P. James, B. Lee, Early stages of crystallisation of lithium disilicate glasses containing P_2O_5 - An NMR study, J. Non-Cryst. Solids 232-234 (1998) 140–146. doi:http://dx.doi.org/10.1016/S0022-3093(98)00381-0.
URL http://www.sciencedirect.com/science/article/pii/S0022309398003810

[17] C. Bischoff, H. Eckert, E. Apel, V. M. Rheinberger, W. Höland, Phase evolution in lithium disilicate glass-ceramics based on non-stoichiometric compositions of a multi-component system: structural studies by ^{29}Si single and double resonance solid state NMR, Phys. Chem. Chem. Phys. 13 (10) (2011) 4540–4551. doi:10.1039/c0cp01440k.

[18] S. Huang, Z. Zujovic, Z. Huang, W. Gao, P. Cao, Crystallization of a high-strength lithium disilicate glass-ceramic: An XRD and solid-state NMR investigation, J. Non-Cryst. Solids 457 (2017) 65–72. doi:10.1016/j.jnoncrysol.2016.11.015.

[19] A. Ananthanarayanan, G. Tricot, G. P. Kothiyal, L. Montagne, A comparative overview of glass-ceramic characterization by MAS-NMR and XRD, Crit. Rev. Solid State Mater. Sci. 36 (4) (2011) 229–241. doi:10.1080/10408436.2011.593643.
URL http://www.tandfonline.com/doi/abs/10.1080/10408436.2011.593643

[20] M. J. Toplis, T. Schaller, ^{31}P MAS NMR study of glasses in the system xNa_2O-(1-x)Al_2O_3-2SiO_2-yP_2O_5, J. Non-Cryst. Solids 224 (1) (1998) 57–68. doi:10.1016/S0022-3093(97)00458-4.

[21] T. Schaller, C. Rong, M. J. Toplis, H. Cho, TRAPDOR NMR investigations of phosphorus-bearing aluminosilicate glasses, J. Non-Cryst. Solids

248 (1) (1999) 19–27.
URL http://www.sciencedirect.com/science/article/pii/S0022309399000988

[22] J. Trebosc, B. Hu, J. Amoureux, Z. Gan, Through-space R^3-HETCOR experiments between spin-1/2 and half-integer quadrupolar nuclei in solid-state NMR, J. Magn. Reson. 186 (2) (2007) 220–227. doi:10.1016/j.jmr.2007.02.015.
URL http://linkinghub.elsevier.com/retrieve/pii/S1090780707000699

[23] G. Tricot, O. Lafon, J. Trebosc, L. Delevoye, F. Méar, L. Montagne, J.-P. Amoureux, Structural characterisation of phosphate materials: new insights into the spatial proximities between phosphorus and quadrupolar nuclei using the D-HMQC MAS NMR technique, Phys. Chem. Chem. Phys. 13 (37) (2011) 16786–16794. doi:10.1039/c1cp20993k.

[24] D. Massiot, F. Fayon, M. Capron, I. King, S. Le Calvé, B. Alonso, J.-O. Durand, B. Bujoli, Z. Gan, G. Hoatson, Modelling one-and two-dimensional solid-state NMR spectra, Magn. Reson. Chem. 40 (1) (2002) 70–76. doi:10.1002/mrc.984.

[25] M. L. Nascimento, L. A. Souza, E. B. Ferreira, E. D. Zanotto, Can glass stability parameters infer glass forming ability?, J. Non-Cryst. Solids 351 (40) (2005) 3296–3308. doi:10.1016/j.jnoncrysol.2005.08.013.
URL http://linkinghub.elsevier.com/retrieve/pii/S002230930500623X

[26] A. K. Yadav, P. Singh, A review of the structures of oxide glasses by Raman spectroscopy, RSC Adv. 5 (83) (2015) 67583–67609. doi:10.1039/C5RA13043C.
URL http://xlink.rsc.org/?DOI=C5RA13043C

[27] T. Fuss, A. Moguš-Milanković, C. S. Ray, C. Lesher, R. Youngman, D. E.

Day, Ex situ XRD, TEM, IR, Raman and NMR spectroscopy of crystallization of lithium disilicate glass at high pressure, J. Non-Cryst. Solids 352 (38) (2006) 4101–4111. doi:10.1016/j.jnoncrysol.2006.06.038.
URL http://linkinghub.elsevier.com/retrieve/pii/S0022309306009513

[28] P. Richet, B. O. Mysen, D. Andrault, Melting and premelting of silicates: Raman spectroscopy and X-ray diffraction of Li_2SiO_3 and Na_2SiO_3, Phys. Chem. Miner. 23 (3) (1996) 157–172.

[29] A. A. Kaminskii, E. Haussühl, H. J. Eichler, J. Hanuza, M. Mączka, H. Yoneda, A. Shirakawa, Lithium silicate, $LiAlSi_4O_{10}$ (petalite) - a novel monoclinic SRS-active crystal, Laser Phys. Lett. 12 (8) (2015) 085002. doi:10.1088/1612-2011/12/8/085002.
URL http://stacks.iop.org/1612-202X/12/i=8/a=085002?key=crossref.4d712c851a779614673482a03e16af7f

[30] I. Alekseeva, O. Dymshits, V. Ermakov, A. Zhilin, V. Petrov, M. Tsenter, Raman spectroscopy quantifying the composition of stuffed β-quartz derivative phases in lithium aluminosilicate glass-ceramics, J. Non-Cryst. Solids 354 (45) (2008) 4932–4939. doi:10.1016/j.jnoncrysol.2008.07.016.
URL http://linkinghub.elsevier.com/retrieve/pii/S0022309308005449

[31] S. Sharma, B. Simons, Raman-study of crystalline polymorphs and glasses of spodumene composition quenched from various pressures, Am. Miner. 66 (1) (1981) 118–126.

[32] L. Popović, B. Manoun, D. de Waal, M. K. Nieuwoudt, J. D. Comins, Raman spectroscopic study of phase transitions in Li_3PO_4, J. Raman Spectrosc. 34 (1) (2003) 77–83. doi:10.1002/jrs.954.
URL http://doi.wiley.com/10.1002/jrs.954

[33] R. Dupree, D. Holland, M. G. Mortuza, The role of small amounts of P_2O_5 in the structure of alkali disilicate glasses, Phys. Chem. Glasses 29 (1) (1988) 18–21.

[34] W. A. Dollase, L. H. Merwin, A. Sebald, Structure of $Na_{3-3x}Al_xPO_4$, x=0 to 0.5, J. Solid State Chem. 83 (1989) 140–149.

[35] J. F. Stebbins, S. Kroeker, S. K. Lee, T. J. Kiczenski, Quantification of five- and six-coordinated aluminum ions in aluminosilicate and fluoride-containing glasses by high-field, high-resolution ^{27}Al NMR, J. Non-Cryst. Solids 275 (1) (2000) 1–6. doi:http://dx.doi.org/10.1016/S0022-3093(00)00270-2.
URL http://www.sciencedirect.com/science/article/pii/S0022309300002702

[36] D. Neuville, L. Cormier, V. Montouillout, D. Massiot, Local Al site distribution in aluminosilicate glasses by ^{27}Al MQMAS NMR, J. Non-Cryst. Solids 353 (2) (2007) 180–184. doi:10.1016/j.jnoncrysol.2006.09.035.
URL http://linkinghub.elsevier.com/retrieve/pii/S002230930601146X

[37] F. Harbach, F. Fischer, Raman Spectra and Optical Absorption Edge of Li_3PO_4 Single Crystals, Phys. Status Solidi B 66 (1) (1974) 237–245.

[38] C. S. Ray, D. E. Day, Determining the Nucleation Rate Curve for Lithium Disilicate Glass by Differential Thermal Analysis, J. Am. Ceram. Soc. 73 (2) (1990) 439–442. doi:10.1111/j.1151-2916.1990.tb06532.x.

[39] G. A. Khater, M. H. Idris, Role of TiO_2 and ZrO_2 on crystallizing phases and microstructure in Li, Ba aluminosilicate glass, Ceramics International 33 (2) (2007) 233–238. doi:10.1016/j.ceramint.2005.08.016.
URL http://linkinghub.elsevier.com/retrieve/pii/S0272884205002701

[40] L. Cormier, O. Dargaud, G. Calas, C. Jousseaume, S. Papin, N. Trcera, A. Cognigni, Zr environment and nucleation role in aluminosilicate glasses, Mater. Chem. Phys. 152 (2015) 41–47. doi:10.1016/j.matchemphys.2014.12.008.
URL http://linkinghub.elsevier.com/retrieve/pii/S0254058414007998

[41] H. R. Fernandes, D. U. Tulyaganov, J. M. F. Ferreira, The role of P_2O_5, TiO_2 and ZrO_2 as nucleating agents on microstructure and crystallization behaviour of lithium disilicate-based glass, J Mater Sci 48 (2) (2013) 765–773. doi:10.1007/s10853-012-6793-4.
URL http://link.springer.com/10.1007/s10853-012-6793-4

[42] A. Gaddam, H. R. Fernandes, D. U. Tulyaganov, M. J. Ribeiro, J. M. F. Ferreira, The roles of P_2O_5 and SiO_2/Li_2O ratio on the network structure and crystallization kinetics of non-stoichiometric lithium disilicate based glasses, J. Non-Cryst. Solids 481 (2018) 512–521. doi:10.1016/j.jnoncrysol.2017.11.034.
URL http://linkinghub.elsevier.com/retrieve/pii/S0022309317306361

[43] A. Ananthanarayanan, G. P. Kothiyal, L. Montagne, B. Revel, MAS-NMR investigations of the crystallization behaviour of lithium aluminum silicate (LAS) glasses containing P_2O_5 and TiO_2 nucleants, J. Solid State Chem. 183 (6) (2010) 1416–1422. doi:10.1016/j.jssc.2010.04.011.
URL http://linkinghub.elsevier.com/retrieve/pii/S0022459610001441

[44] F. Fayon, C. Duée, T. Poumeyrol, M. Allix, D. Massiot, Evidence of Nanometric-Sized Phosphate Clusters in Bioactive Glasses As Revealed by Solid-State ^{31}P-NMR, J. Phys. Chem. C 117 (5) (2013) 2283–2288. doi:10.1021/jp312263j.
URL http://pubs.acs.org/doi/abs/10.1021/jp312263j

[45] O. Dargaud, L. Cormier, N. Menguy, G. Patriarche, Multi-scale structuration of glasses: Observations of phase separation and nanoscale heterogeneities in glasses by Z-contrast scanning electron transmission microscopy, J. Non-Cryst. Solids 358 (10) (2012) 1257–1262. doi:10.1016/j.jnoncrysol.2012.02.026.
URL http://linkinghub.elsevier.com/retrieve/pii/S0022309312001196

[46] S. K. Lee, J. F. Stebbins, Al–O–Al and Si–O–Si sites in framework aluminosilicate glasses with Si/Al= 1: quantification of framework disorder, J. Non-Cryst. Solids 270 (1) (2000) 260–264. doi:10.1016/S0022-3093(00)00089-2.

[47] Extent of intermixing among framework units in silicate glasses and meltsdoi:10.1016/S0016-7037(01)00775-X.

[48] S. Wegner, L. van Wüllen, G. Tricot, The structure of aluminophosphate glasses revisited: Application of modern solid state NMR strategies to determine structural motifs on intermediate length scales, J. Non-Cryst. Solids 354 (15-16) (2008) 1703–1714. doi:10.1016/j.jnoncrysol.2007.10.034.
URL http://linkinghub.elsevier.com/retrieve/pii/S0022309307012458

[49] M. Toplis, G. Libourel, M. Carroll, The role of phosphorus in crystallization processes of basalt - an experimental study, Geochim. Cosmochim. Acta 58 (2) (1994) 797–810. doi:10.1016/0016-7037(94)90506-1.

[50] M. Bengisu, R. K. Brow, A. Wittenauer, Glasses and glass-ceramics in the SrO-–TiO_2—Al_2O_3—SiO_2-–B_2O_3 system and the effect of P_2O_5 additions, J Mater Sci 43 (10) (2008) 3531–3538. doi:10.1007/s10853-008-2541-1.
URL http://link.springer.com/10.1007/s10853-008-2541-1

[51] C. S. Ray, D. E. Day, An Analysis of Nucleation-Rate Type of Curves in Glass as Determined by Differential Thermal Analysis, J. Am. Ceram. Soc

80 (12) (1997) 3100–3108.

URL http://onlinelibrary.wiley.com/doi/10.1111/j.1151-2916.
730 1997.tb03238.x/full

Figures

Glass	SiO_2	Al_2O_3	Li_2O	P_2O_5	R	T_g(°C)	T_x(°C)	T_c(°C)	T_x-T_g(°C)
LAS0-P0	74.4	0.3	25.3	0.01	0.01	483	659	764	176
LAS0-P1	73.6	0.2	25.1	1.1	0.01	477	606	635	129
LAS0.2-P0	75.7	4.6	19.7	0.02	0.23	507	660	832	153
LAS0.2-P1	74.3	4.2	20.7	0.8	0.20	509	592	646	83
LAS0.4-P0	74.5	7.4	18.1	0.01	0.41	536	651	770	115
LAS0.4-P1	75.0	7.6	16.4	1.0	0.46	548	617	639	69
LAS0.7-P0	73.6	10.8	15.6	0.01	0.69	594	559	769	65
LAS0.7-P1	73.8	10.2	15.0	1.0	0.68	614	708	840	94
LAS1-P0	74.0	13.2	12.8	0.003	1.03	748	852	922	104
LAS1-P1	73.7	13.0	12.5	0.79	1.04	736	936	1005	200
LAS1.3-P0	74.1	14.7	11.2	0.01	1.32	770	1080	1222	310
LAS1.3-P1	75.0	14.6	9.4	0.96	1.55	778	/	1234	/

Table 1: Compositions (mol%) analyzed by EPMA and FAES for the glasses investigated in this study. R=$\frac{Al_2O_3}{Li_2O}$. T_g is the glass transition temperature and T_x is the temperature of the first crystallization peak determined from the DSC curves. The error in the determination of T_g, T_x and T_c is estimated close to ± 2 °C.

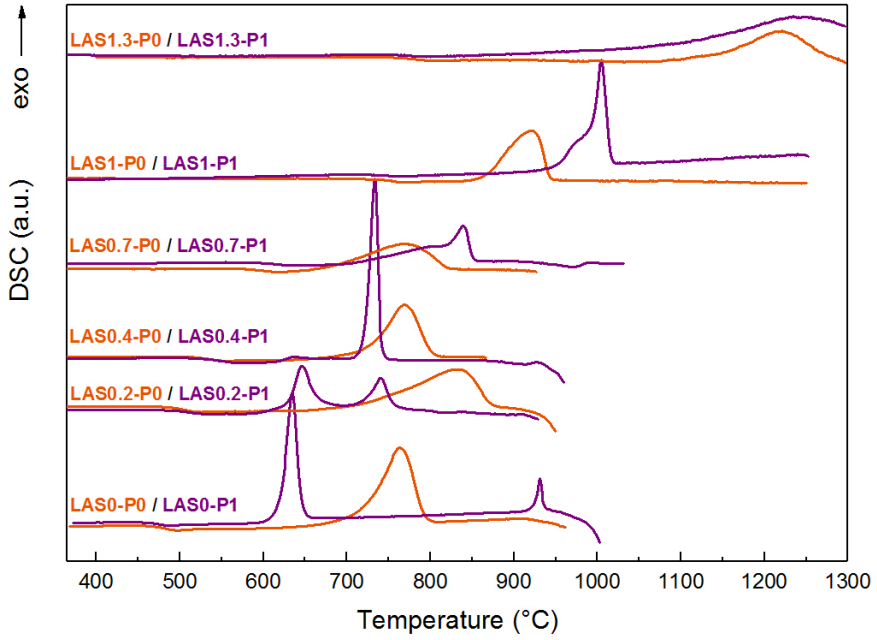

Figure 1: Differential scanning calorimetry curves of the glasses without (orange) P_2O_5 and with (purple) 1 mol% P_2O_5

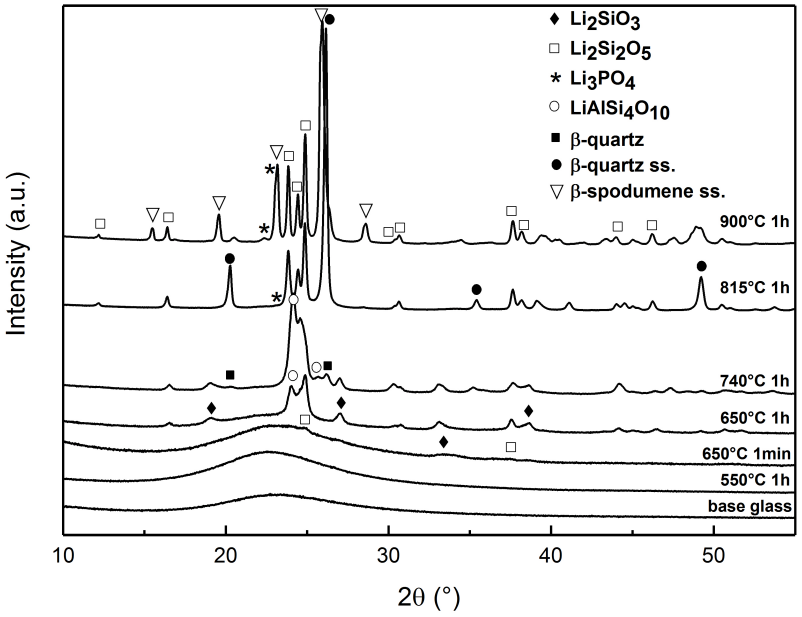

(a)

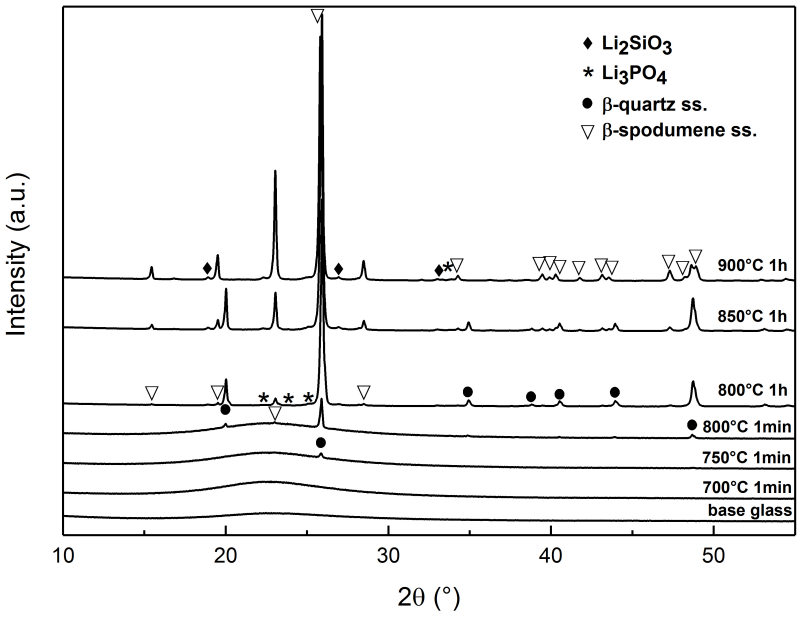

(b)

Figure 2: XRD patterns of the compositions LAS0.2-P1 (a) and LAS0.7-P1 (b) annealing at different temperatures and times

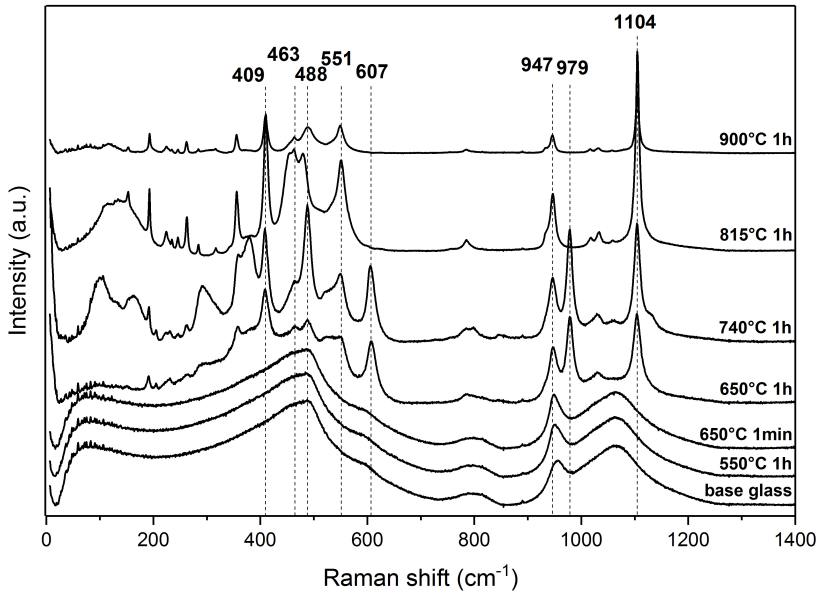

(a)

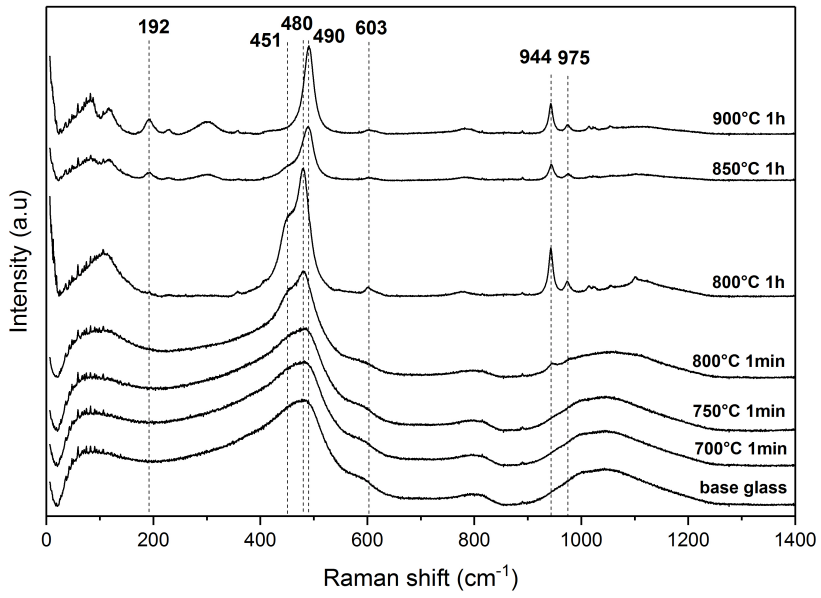

(b)

Figure 3: RAMAN spectra of LAS0.2-P1 (a) and LAS0.7-P1 (b) annealed at different temperatures and times

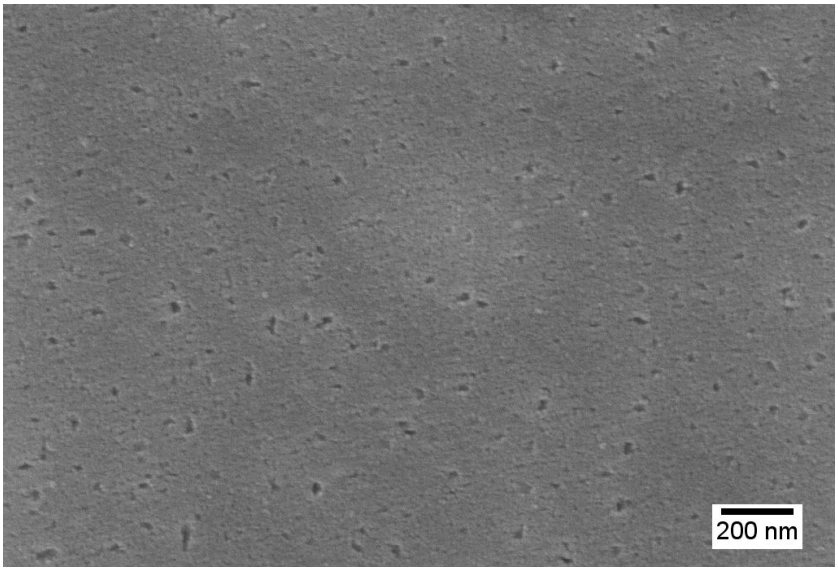

(a)

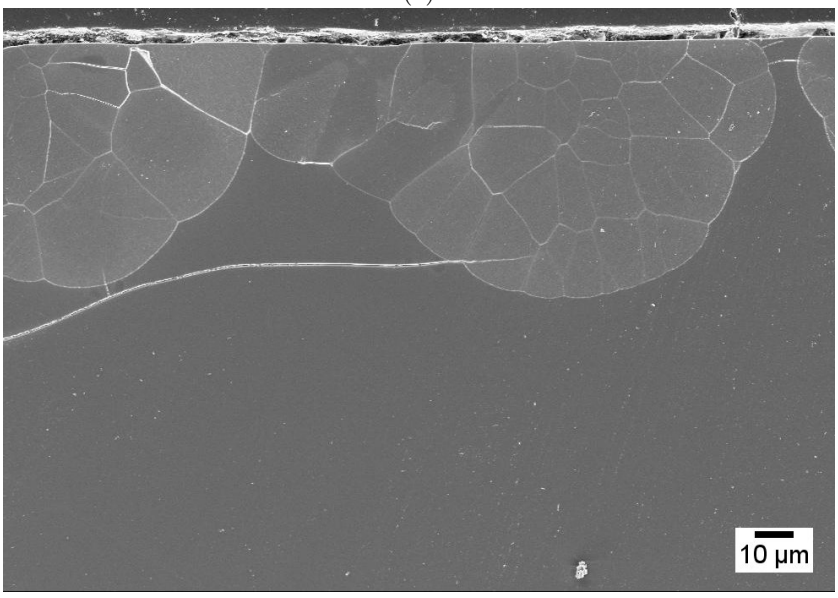

(b)

Figure 4: SEM image of samples polished then etched with 1 % HF for 30 seconds of (a) LAS0.2-P1 annealed at 650 °C for 1 minute, (b) LAS0.7-P1 annealed at 800 °C for 1 minute

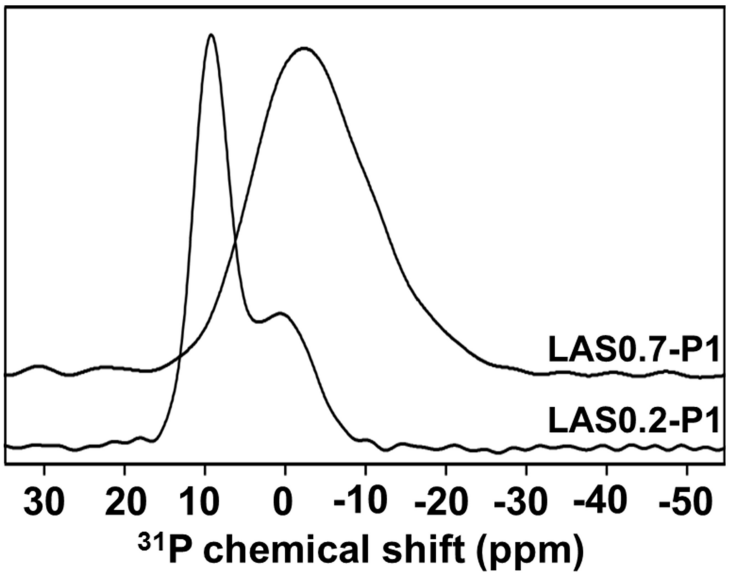

(a)

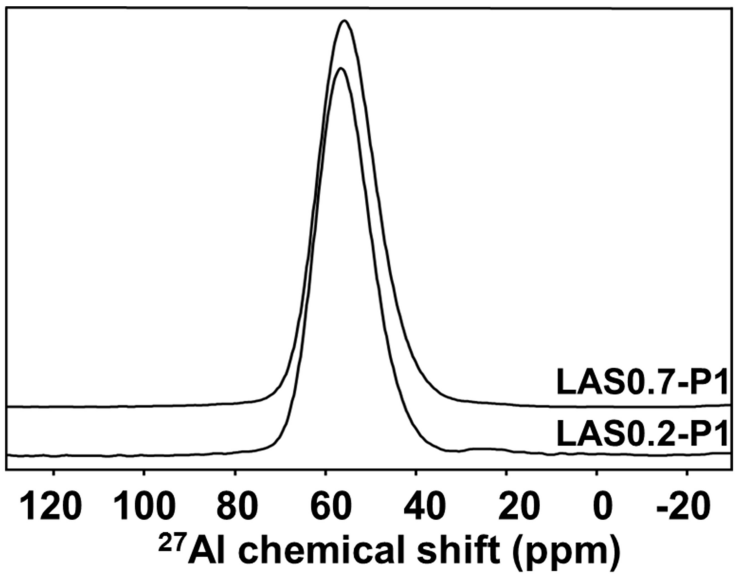

(b)

Figure 5: (a) ^{31}P MAS-NMR spectra recorded at 9.4 T, (b) ^{27}Al MAS-NMR spectra recorded at 18.8 T of as-cast glasses LAS0.2-P1 and LAS0.7-P1

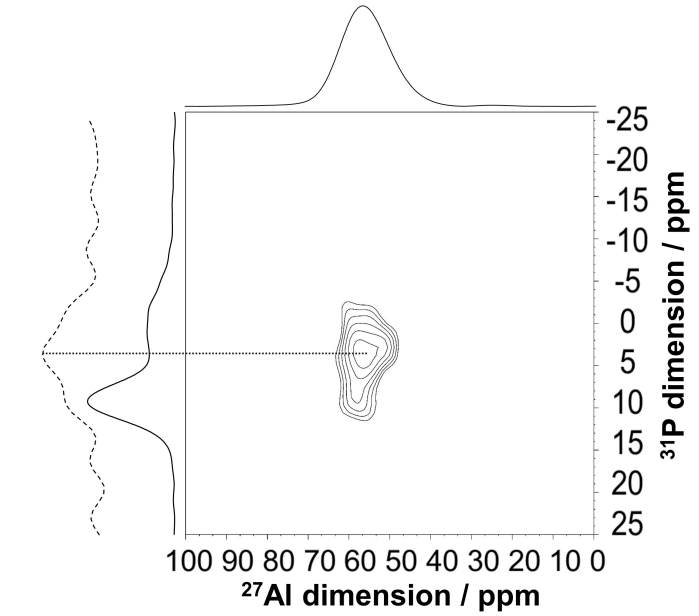

(a)

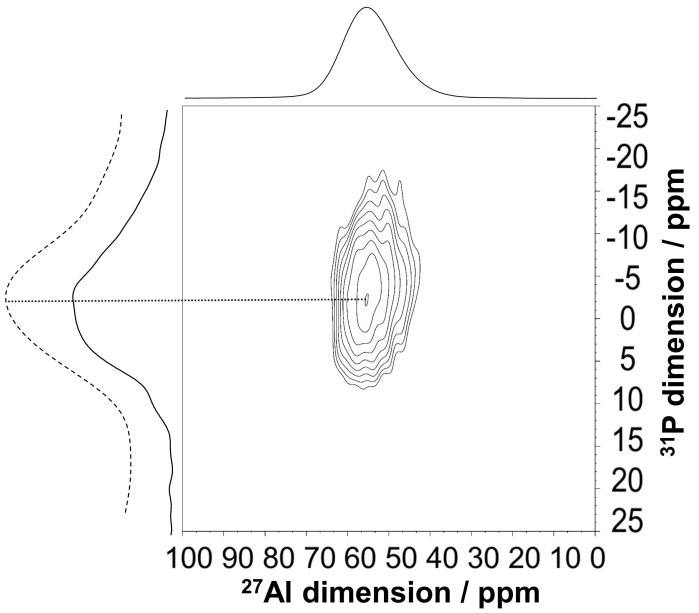

(b)

Figure 6: ^{27}Al{^{31}P} D-HMQC spectra recorded at 18.8 T of as-cast glasses LAS0.2P1 (a) and LAS0.7-P1 (b). The dashed lines are the ^{31}P projections of the 2D spectra.

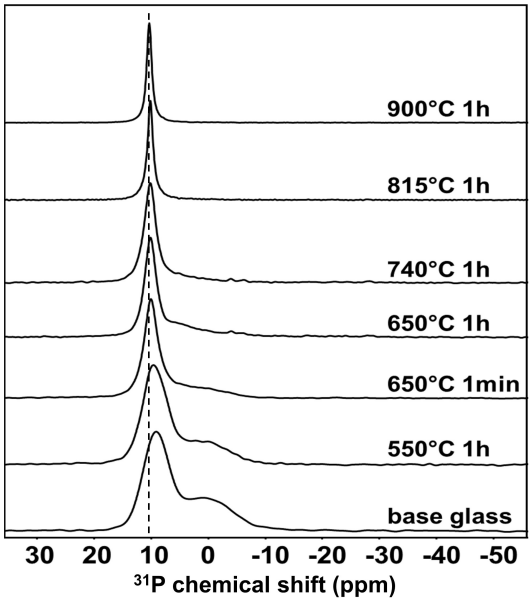

(a)

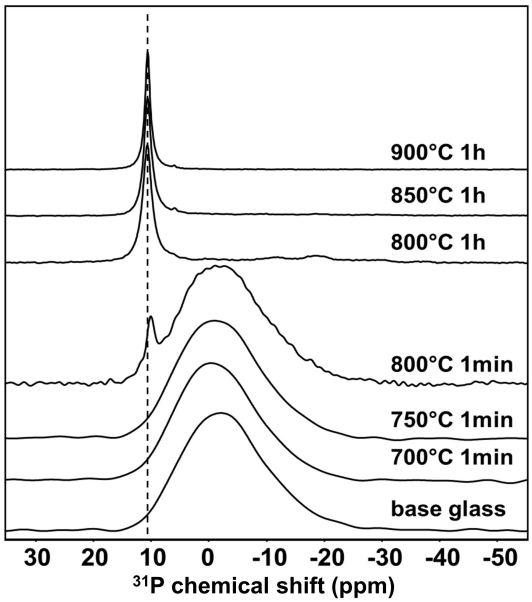

(b)

Figure 7: ^{31}P MAS-NMR spectra recorded at 9.4 T of LAS0.2-P1 (a) and LAS0.7-P1 (b) annealed at different temperatures and times